

See discussions, stats, and author profiles for this publication at: <https://www.researchgate.net/publication/281326033>

A Comparative Insight into Amprenavir Resistance of Mutations V32I, G48V, I50V, I54V and I84V in HIV-1 Protease Based on Thermodynamic Integration and MM-PBSA Methods

ARTICLE *in* JOURNAL OF CHEMICAL INFORMATION AND MODELING · AUGUST 2015

Impact Factor: 3.74 · DOI: 10.1021/acs.jcim.5b00173

CITATIONS

2

READS

31

5 AUTHORS, INCLUDING:



Jianzhong Chen

Shandong Jiaotong University

20 PUBLICATIONS 136 CITATIONS

[SEE PROFILE](#)



John Z.H. Zhang

East China Normal University, New York Univ...

297 PUBLICATIONS 7,781 CITATIONS

[SEE PROFILE](#)

A Comparative Insight into Amprenavir Resistance of Mutations V32I, G48V, I50V, I54V, and I84V in HIV-1 Protease Based on Thermodynamic Integration and MM-PBSA Methods

Jianzhong Chen,^{*,†} Xingyu Wang,[‡] Tong Zhu,^{*,§} Qinggang Zhang,^{||} and John Z. H. Zhang^{‡,§}

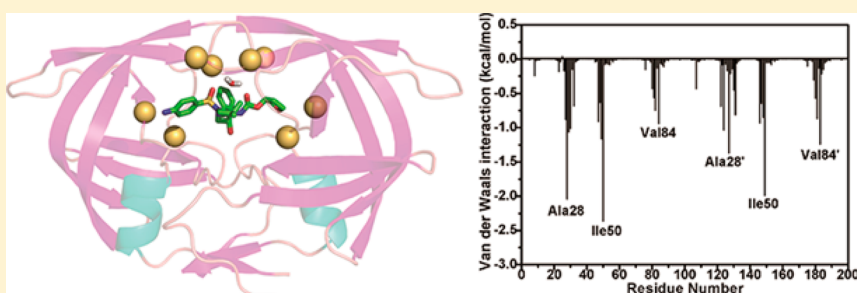
[†]School of Science, Shandong Jiaotong University, Jinan 250357 China

[‡]NYU–ECNU Center for Computational Chemistry at NYU Shanghai, Shanghai 200062, China

[§]State Key Laboratory of Precision Spectroscopy, Institute of Theoretical and Computational Science, East China Normal University, Shanghai 200062, China

^{||}College of Physics and Electronic Science, Shandong Normal University, Jinan 250014, China

Supporting Information



ABSTRACT: Drug resistance of mutations V32I, G48V, I50V, I54V, and I84V in HIV-1 protease (PR) was found in clinical treatment of HIV patients with the drug amprenavir (APV). In order to elucidate the molecular mechanism of drug resistance associated with these mutations, the thermodynamic integration (TI) and molecular mechanics Poisson–Boltzmann surface area (MM-PBSA) methods were applied to calculate binding free energies of APV to wild-type PR and these mutated PRs. The relative binding free energy differences from the TI calculations reveal that the decrease in van der Waals interactions of APV with mutated PRs relative to the wild-type PR mainly drives the drug resistance. This result is in good agreement with the previous experimental results and is also consistent with the results from MM-PBSA calculations. Analyses based on molecular dynamics trajectories show that these mutations can adjust the shape and conformation of the binding pocket, which provides main contributions to the decrease in the van der Waals interactions of APV with mutated PRs. The present study could provide important guidance for the design of new potent inhibitors that could alleviate drug resistance of PR due to mutations.

INTRODUCTION

The worldwide spread of acquired immunodeficiency syndrome (AIDS) has been a major clinical challenge for more than 30 years. Numerous studies have suggested that HIV-1 protease (PR) is one of the three significant enzymes that play a key role in the life cycle of the HIV virus. This protein is responsible for the cleavage of the *gag* and *pol* nonfunctional polypeptides into mature and functional HIV viral particles that can infect human host cells.^{1,2} Structurally, PR is a *C*₂-symmetric homodimer composed of two identical 99 amino acid monomers (Figure 1A). The active site of PR, consisting of two conserved strands (D25/D25'-T26/T26'-G27/G27'), is located in the interface between the two monomers. The flaps located at the top of PR undergo structural changes upon binding of inhibitors and substrates.^{3,4} Binding of inhibitors to PR can inhibit the activity of PR and hold back the formation of mature and functional HIV viral particles.^{5–7} Thus, PR is an important target of drug design for anti-HIV therapeutics.

To date there are 10 HIV-1 PR inhibitors (PIs) that have been approved by the U.S. Food and Drug Administration (FDA). All of these inhibitors were successfully developed by structure-assisted drug design.^{8,9} Among these, amprenavir (APV) is the first drug containing both a sulfonamide and a hydroxyethylamine core that mimics the transition state of the enzyme (Figure 1B). Compared with the first-generation inhibitor saquinavir, the addition of the sulfonamide group strengthens the water solubility of APV.¹⁰ Previous studies on the crystal structure of the APV–PR complex showed that APV has potent PR inhibition ability with a *K*_i value of 0.15 nM.^{11–13} However, drug resistance caused by mutations limits the efficacy of APV in clinical treatment. Thus, reducing the level of drug resistance due to mutations is a great challenge in curing HIV patients.

Received: March 30, 2015

Published: August 28, 2015

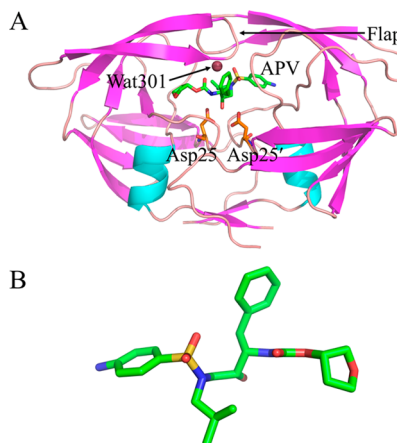


Figure 1. Molecular structures of (A) the APV–PR complex and (B) amprenavir (APV). The APV–PR complex is displayed in cartoon mode, and APV and Asp25/Asp25' are shown in stick mode.

Mutations of PR can reduce its binding affinity with inhibitors.^{14–17} Some conservative mutations of hydrophobic residues, such as V32I, I50V, I54V, V82A, and I84V, were observed in experimental and clinical treatments to produce drug resistance toward PIs.^{18–22} Residue mutations can change the shape of the binding cavity and consequently reduce the binding affinity. Work by Shen et al.¹² suggested that mutations V32I, I50V, I54V, and I84V weaken the PR inhibition ability of APV. The mutation V32I increases the size of the side chain of residue 32 and has been found in ~20% of patients treated with APV. Residues Ile50 and Ile54 are located in the flaps of PR, which are significant for catalysis of the substrate and binding of inhibitors.^{11,23} Mutations of the flap region can also change the structural stability of PR or the binding ability of inhibitors.^{23–26} Theoretical studies by Alcaro et al.²⁶ showed that the mutations V82A, I84V, M46I, and L76V can decrease the stability of PR–inhibitor complexes, thereby causing drug resistance. Previous studies also showed that Ile50 produces strong and direct interactions with inhibitors while Ile54 does not form direct interactions with inhibitors,^{27–29} which means that the mutations I50V and I54V should have different mechanisms of resistance toward APV. The mutation I84V, which occurs in the binding pocket and shortens the size of residue 84, greatly weakens the binding affinity of APV to PR. Additionally, the mutation G48V, which occurs in the flaps and increases the size of the side chain, was found to produce obvious drug resistance toward several current inhibitors.^{30–32} Thus, it is important to clarify the drug resistance mechanisms of these different types of mutations on APV at the atomic level for the design of potent PIs.

Molecular dynamics (MD) simulations and free energy calculations are efficient tools to investigate many thermodynamic properties of proteins and protein–inhibitor interactions.^{33–47} In this work, the mutations V32I, G48V, I50V, I54V, and I84V of PR were chosen to probe their drug resistance mechanisms toward APV at the atomic level. To achieve this aim, MD simulations and the molecular mechanics Poisson–Boltzmann surface area (MM-PBSA)^{48–51} and thermodynamic integration (TI) methods^{52–54} were combined to perform a systematic comparative study. In view of the importance of conformational changes in drug design, cross-correlation analysis and free energy landscape calculations were also performed to explore the changes in the internal dynamics

of PR induced by mutation. This study can be expected to provide significant a molecular basis and dynamics information for the design of potent PIs inhibiting drug resistance caused by mutations.

METHODS

System Preparation. The crystal structure of the wild-type APV–PR complex was obtained from the Protein Data Bank (PDB ID 3EKV).⁵⁵ To keep consistency, this crystal structure was used as the template to construct single-mutant complexes. Because of the important effect of Asp25/Asp25' on PR–ligand binding,^{56,57} a monoprotonated state was assigned to the oxygen atom OD2 of Asp25' of PR using the program PROPKA.^{58,59} All water molecules in the crystal structure were retained. The Leap module in Amber12 was used to add all of the missing hydrogen atoms and construct the mutated PR structures.⁶⁰ The Amber 99SB force field was assigned for PR.⁶¹ The structure of APV was optimized with the Gaussian 09 program⁶² at the HF/6-31G* level, and then restrained electrostatic potential (RESP) charges and the general Amber force field (GAFF) were assigned for the optimized structure.⁶³ The complex was solvated in a truncated octahedral box of TIP3P water molecules with a 12.0 Å buffer along each dimension.⁶⁴ Cl[−] counterions were added to neutralize the system.

MD Simulations in Water. For each system, energy minimization and MD simulation were performed using the Sander module in Amber12. A two-step, extensive energy minimization process based on the steepest descent method followed by the conjugate gradient algorithm were carried out to relieve bad contacts and to direct each system toward energetically favorable conformations. First, water molecules and counterions were relaxed by restraining the complex with a harmonic constant of 100 kcal/mol·Å^{−2}. Second, the restraint was removed to allow all of the atoms to move freely. After minimization, each system was gently heated from 0 to 300 K in 500 ps at constant volume and equilibrated at 300 K for another 500 ps. Finally, a 120 ns MD simulation without any restrictions was performed at constant pressure, and the coordinates of atoms were saved every 2 ps. During the MD simulation, all bonds involving hydrogen atoms were constrained using the SHAKE algorithm,⁶⁵ and a time step of 2 fs was adopted. The temperature was controlled using the Langevin thermostat⁶⁶ with a collision frequency of 2.0 ps^{−1}. The particle mesh Ewald (PME) method was applied to treat the long-range electrostatic interactions.^{67,68} The cutoff distances for the long-range electrostatic and van der Waals interactions were set to 12.0 Å.

MM-PBSA Method. The MM-PBSA method was used to calculate the binding affinity of APV to wild-type (WT) and mutated PRs.^{49,50} For each simulated system, 500 snapshots were extracted from the last 20 ns of the MD trajectory at intervals of 40 ps for calculations. In the MM-PBSA scheme, the binding free energy (ΔG) is computed using the following equation:

$$\Delta G = \Delta E_{\text{ele}} + \Delta E_{\text{vdW}} + \Delta G_{\text{pol}} + \Delta G_{\text{nonpol}} - T\Delta S \quad (1)$$

The first two terms (ΔE_{ele} and ΔE_{vdW}) represent the electrostatic and van der Waals interactions in the gas phase, respectively. The third term (ΔG_{pol}) is the polar solvation free energy, which was calculated by solving the Poisson–Boltzmann equation. The fourth term (ΔG_{nonpol}) represents

the nonpolar solvation energy, which can be calculated using the empirical equation $\Delta G_{\text{nonpol}} = \gamma \times \text{SASA} + \beta$, in which SASA represents the solvent-accessible surface area and the values of γ and β were set to 0.00542 kcal/mol·Å⁻² and 0.92 kcal/mol, respectively.⁶⁹ The contribution of the entropy change to the binding affinity ($-T\Delta S$) can be calculated by normal mode analysis.⁷⁰

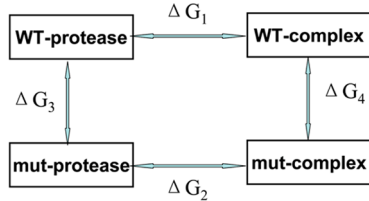
Cross-Correlation Analysis. To investigate the effect of residue mutation on the conformation and internal dynamics changes of PR, the cross-correlation matrix elements C_{ij} , which reflect the fluctuation of coordinates of the C_α atoms relative to their average positions, were calculated from the last 20 ns of the MD trajectory for each system using the following equation:

$$C_{ij} = \frac{\langle \Delta \mathbf{r}_i \cdot \Delta \mathbf{r}_j \rangle}{(\langle \Delta \mathbf{r}_i^2 \rangle \langle \Delta \mathbf{r}_j^2 \rangle)^{1/2}} \quad (2)$$

where the angle brackets represent a time average over the equilibrated simulation time and $\Delta \mathbf{r}_i$ indicates the displacement vector from the mean position for the C_α atom in the i th residue.⁷¹ The value of C_{ij} ranges from -1 to 1. A positive C_{ij} value represents a correlated motion of the C_α atoms of the i th and j th residues, while a negative value of C_{ij} describes an anticorrelated motion.

Thermodynamic Integration Calculations. In clarifying the drug resistance mechanism of mutated PR on inhibitors, the most valuable information should come from the relative difference in binding free energy between two states ($\Delta\Delta G$). Thermodynamic integration (TI) is an efficient tool for calculating the relative energy difference on the basis of MD simulations. In this kind of calculation, the scheme shown in

Scheme 1. Thermodynamic Cycle Used to Perform Thermodynamic Integration



Scheme 1) was mostly used,^{17,40,72,73} and the value of $\Delta\Delta G$ was calculated as

$$\Delta\Delta G = \Delta G_2 - \Delta G_1 = \Delta G_4 - \Delta G_3 \quad (3)$$

where ΔG_1 and ΔG_2 represent the binding free energies of an inhibitor to two different protein states (the WT and mutated

structures, respectively) while ΔG_3 and ΔG_4 represent the transformation from one protein to the other when solvated in water (ΔG_3) or bound to an inhibitor (ΔG_4).

The relative binding free energies can be calculated using the following equation:

$$\Delta G = \int_0^1 \left\langle \frac{\partial V(\lambda)}{\partial \lambda} \right\rangle_\lambda d\lambda \quad (4)$$

where λ is the coupling parameter, V is the λ coupling potential function, the integration limits 0 and 1 represent two different states that correspond to the WT and mutated PR, respectively, and the angle brackets represent a Boltzmann-weighted average. The integral in eq 4 is solved numerically using several simulations with different windows of fixed λ values ranging from 0 to 1 according to eq 5:

$$\Delta G = \sum_{i=1}^n W_i \left\langle \frac{\partial V}{\partial \lambda} \right\rangle_{\lambda_i} \quad (5)$$

The values of λ and their corresponding weights W_i can be assigned by using the Gaussian quadratic formula. The potential functions $V(0)$ for $\lambda = 0$ and $V(1)$ for $\lambda = 1$ correspond to the WT and mutated PR, respectively. The TI calculation was achieved for each λ in three steps: (1) charge removal from the side-chain atoms of the WT residue being mutated; (2) change of the WT residue into the mutated residue (without electrostatic interaction); and (3) charge addition to the side-chain atoms of the mutated residue. Figure S1 illustrates the changes in residues used in the mutations. In the TI calculations, the soft-core potential was activated only during the second step to treat the disappearance and appearance of atoms involved in the mutation. The sampling space was characterized by 12 different λ values. For each λ value, six separate 2 ns MD simulations were performed on the WT and mutated PR. In all of the calculations, the values of λ and their corresponding weights were taken from the Amber12 package (Table S1); those values were used successfully in previous studies to study drug resistance of PR mutations.^{17,40}

RESULTS AND DISCUSSION

Revelation of Drug Resistance Based on TI Calculations. In this study, a series of MD simulations were carried out to perturb WT PR into its five mutated states. The relative binding free energies ($\Delta\Delta G$) for these five mutations are summarized in Table 1. As can be seen, the rank of predicted relative binding free energies is in agreement with the experimentally determined one. One can also observe that all five mutations lead to a decrease in binding affinity, which means that these five mutations all generate drug resistance toward APV.

Table 1. Relative Binding Free Energies Calculated by Thermodynamic Integration^a

PR	$\Delta\Delta G_{s1}$ (step 1)	$\Delta\Delta G_{s2}$ (step 2)	$\Delta\Delta G_{s3}$ (step 3)	$\Delta\Delta G$ (total)	ΔG_{exp}^b	$\Delta\Delta G_{\text{exp}}^c$
WT					-13.35	
V32I	-0.17 ± 0.29	1.74 ± 5.02	-0.09 ± 0.16	1.48 ± 5.12	-12.14	1.21
G48V	0.06 ± 0.34	0.57 ± 4.11	0.08 ± 0.42	0.71 ± 4.01	-12.62	0.73
I50V	-0.18 ± 0.22	2.36 ± 4.91	0.12 ± 0.48	2.30 ± 4.65	-11.44	1.91
I54V	0.02 ± 0.14	0.29 ± 4.08	0.03 ± 0.36	0.34 ± 4.42	-12.73	0.62
I84V	0.05 ± 0.18	0.64 ± 4.45	0.11 ± 0.18	0.80 ± 4.58	-12.51	0.84

^aAll values are in kcal/mol. Errors labeled by the ± signs represent standard errors. ^bThe experimental values were derived from the experimental K_i values in refs 32 and 55 using the equation $\Delta G_{\text{exp}} = -RT \ln K_i$. ^c $\Delta\Delta G_{\text{exp}} = \Delta G_{\text{mutated}} - \Delta G_{\text{WT}}$.

Table 2. Energy Analysis for Binding of APV to WT PR and Mutated PRs As Obtained by the MM-PBSA Method^a

energy	WT	V32I	G48V	I50V	I54V	I84V
ΔE_{ele}	-47.04 ± 0.56	-42.94 ± 0.41	-42.69 ± 0.31	-42.38 ± 0.62	-45.97 ± 0.65	-42.98 ± 0.45
ΔE_{vdW}	-63.85 ± 0.21	-61.52 ± 0.19	-62.24 ± 0.10	-60.35 ± 0.18	-61.55 ± 0.11	-61.45 ± 0.10
ΔG_{pol}	75.16 ± 0.49	70.65 ± 0.52	70.18 ± 0.47	70.45 ± 0.78	73.58 ± 0.66	71.11 ± 0.42
ΔG_{nonpol}	-6.99 ± 0.02	-7.02 ± 0.01	-6.95 ± 0.01	-6.81 ± 0.01	-6.83 ± 0.01	-7.09 ± 0.01
$\Delta G_{\text{ele+pol}}^b$	28.12 ± 0.50	27.71 ± 0.49	27.49 ± 0.42	28.07 ± 0.69	27.61 ± 0.68	28.13 ± 0.39
$-T\Delta S$	27.68 ± 0.23	27.52 ± 0.12	27.92 ± 0.19	27.01 ± 0.18	26.88 ± 0.15	27.02 ± 0.18
ΔG_{bind}^c	-15.04	-13.31	-13.78	-12.08	-13.89	-13.39
ΔG_{exp}^d	-13.35	-12.14	-12.62	-11.44	-12.73	-12.51

^aAll values are in kcal/mol. Errors labeled by the \pm signs represent standard errors. ^b $\Delta G_{\text{ele+pol}} = \Delta E_{\text{ele}} + \Delta G_{\text{pol}}$. ^c $\Delta G_{\text{bind}} = \Delta E_{\text{ele}} + \Delta E_{\text{vdW}} + \Delta G_{\text{pol}} + \Delta G_{\text{nonpol}} - T\Delta S$. ^dThe experimental values were derived from the experimental K_i values in refs 32 and 55 using the equation $\Delta G_{\text{exp}} = -RT \ln K_i$.

According to Table 1, the mutation I50V results in the biggest change in the binding free energy relative to WT PR ($\Delta\Delta G = 2.30$ kcal/mol), which means that I50V produces the strongest resistance toward APV. The binding free energy of APV to the V32I mutant is increased by 1.48 kcal/mol, which indicates that V32I also induces strong resistance toward APV. The free energy differences for binding to APV for the mutations G48V, I54V, and I84V relative to WT PR are 0.71, 0.34 and 0.80 kcal/mol, respectively, which are smaller than those for I50V and V32I. The drug resistance of I54V toward APV is the weakest. This result is rational because many previous studies proved that residue Ile54 does not produce strong and direct interactions with APV. For the mutations V32I, G48V, I50V, and I84V, structural changes in the hydrophobic side chain should be responsible for their main drug resistance toward APV.

To further probe the origin of drug resistance induced by mutation, relative free energy differences for the three separate steps of TI ($\Delta\Delta G_{s1}$, $\Delta\Delta G_{s2}$, and $\Delta\Delta G_{s3}$) were also computed, and the results are listed in Table 1. $\Delta\Delta G_{s1}$ and $\Delta\Delta G_{s3}$ are caused by charge removal in step 1 and charge addition in step 3, respectively. These two energy differences should reflect the changes in polar interactions between the protein and ligand. The second step of the TI calculation involves only the change in the van der Waals interactions of the protein with ligand induced by mutation. For the mutations V32I and I50V, the sums of $\Delta\Delta G_{s1}$ and $\Delta\Delta G_{s3}$ are -0.26 and -0.06 kcal/mol respectively, which means that the polar interaction changes do not provide any contributions to their drug resistance toward APV. In the case of G48V, I54V, and I84V, the polar interactions provide only very weak contributions to drug resistance. For the second step, the relative free energy differences are $\Delta\Delta G_{s2} = 1.74$, 0.57, 2.36, 0.29, and 0.64 kcal/mol for the mutations V32I, G48V, I50V, I54V, and I84V, respectively, which are much larger than the sums of $\Delta\Delta G_{s1}$ and $\Delta\Delta G_{s3}$. Figure S3 depicts the $dV/d\lambda$ curves during the transformation of the inhibitor–PR complexes from the WT to the mutated state in the TI calculations. As can be seen, the van der Waals transformation in each complex shows the biggest fluctuations of $dV/d\lambda$, and the free energy curve for step 2 is the one that looks the most “bumpy”. This implies again that the main contribution to the binding free energy difference stems from the change in the van der Waals interactions, and thus, the change in the van der Waals interactions induced by the change in the residue side chain is a main force driving drug resistance of mutations toward APV. The above results and analyses basically agree with those of previous experimental studies.⁵⁵

Revelation of Drug Resistance Based on MM-PBSA Calculations. To obtain further energy information concern-

ing the impact of mutations on drug resistance, 120 ns MD simulations followed by MM-PBSA calculations were performed on six APV–protein systems. Root-mean-square deviation (RMSD) calculations for the backbone heavy atoms of WT PR and all of the mutated complexes showed that the simulations converged after ~ 10 ns, thus yielding stable trajectories for all of the systems (Figure S2). The absolute free energies for binding of APV to WT PR and the mutated PRs and separate free energy component contributions were calculated using the MM-PBSA method on the basis of 500 frames extracted from the last 20 ns of each MD trajectory at intervals of 40 ps.

According to Table 2, the rank of the absolute binding free energies predicted by the MM-PBSA method agrees well with the experimentally determined one, which shows that the current energy analysis is reliable. Table 2 indicates that contributions favoring APV binding are those from the van der Waals interactions (ΔE_{vdW}) and nonpolar interactions (ΔG_{nonpol}). Although the electrostatic interactions between APV and PR (ΔE_{ele}) also contribute favorable force to the binding, this favorable force is completely countered by the stronger and unfavorable polar solvation free energy (ΔG_{pol}), generating an unfavorable total polar interaction ($\Delta G_{\text{ele+pol}}$). The entropy contribution ($-T\Delta S$), which depends on the changes of motional freedom induced by the binding of APV, also weakens the binding.

One can observe from Table 2 that mutations produce an obvious impact on the binding of APV to PR. The free energies for binding of APV to the V32I, G48V, I50V, I54V, and I84V mutants are increased by 1.73, 1.26, 2.96, 1.15, and 1.65 kcal/mol, respectively, relative to WT PR, which suggest that all five of these mutations produce drug resistance toward APV. The polar interactions ($\Delta G_{\text{ele+pol}}$) of APV with the five mutated PRs are very close to that of APV with WT PR, indicating that this interaction does not provide contributions to drug resistance. The changes in nonpolar solvation free energy and entropy during mutation are also very small. However, Table 2 shows that van der Waals interactions of APV with the mutated PR are changed by 2.33, 1.61, 3.50, 2.30, and 2.40 kcal/mol for V32I, G48V, I50V, I54V, and I84V, respectively, which indicates that the drug resistance of these five mutations is mainly derived from changes in the van der Waals interactions. These results are consistent with those of the TI calculations and agree well with previous studies.^{12,74–77}

Internal Dynamics Changes in PR. Root-mean-square fluctuations (RMSFs) of C_α atoms can provide direct insight into the flexibility of a protein. As can be seen from Figure 2, the residues near the catalytic site Asp25/Asp25' show a high degree of rigidity in the WT and mutated PRs, which is

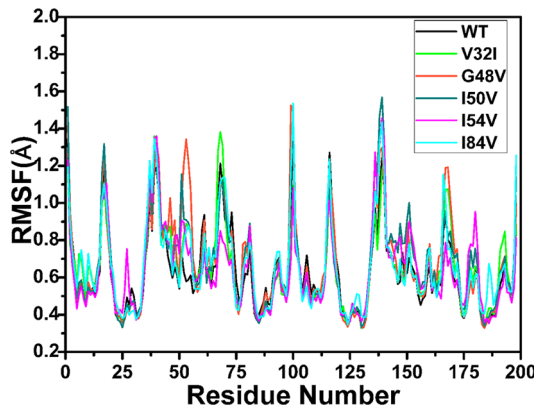


Figure 2. Root-mean-square fluctuations (RMSFs) of $\text{C}\alpha$ atoms of WT and mutated PR.

expected because the catalytic function of these residues presumably requires a well-defined, stable three-dimensional structure. Besides, it is noteworthy that all five of these mutations highly increase the RMSF values of the flaps involving residues 40–55/40'-50', especially the mutations G48V, I50V, and I54V, which suggests that the flexibility of the flaps is significantly strengthened by the mutations. The conformation changes near the flaps may lead to rearrangement of the residues, which would affect the interactions of the flaps with APV and may be responsible for the drug resistance. Additionally, the mutation V32I obviously increases the RMSF values near residues 68/68', while I84V results in an increase in the RMSF near residue 68' and I54V also strengthens the flexibility of the region near residue 81'.

To further probe the difference in internal dynamics of PR caused by mutations, the cross-correlation matrices after equilibration of the MD simulations were computed using the Cpptraj program⁷⁸ in Amber12, and the results are displayed in Figure 3. Highly positive regions (red and yellow) and negative ones (dark blue) describe strongly correlated and anticorrelated motions, respectively. Overall, except for the diagonal regions describing the correlated motion of a specific residue relative to itself, few highly correlated motions are observed. However, the changes in anticorrelated movements induced by the mutations are obvious, especially for the mutation I84V.

In the APV–WT PR complex (Figure 3A), binding of APV produces an obvious correlated motion and weak anticorrelated motion in region R1, which reflects the conformation changes of the flap and its nearby region. According to Figure 3A, an obvious anticorrelated movement is found in region R2, which indicates the anticorrelated motion of residues 60–80 relative to the N-terminus of chain B.

Compared with Figure 3A, the five mutations generate obvious changes in motional modes of PR. One can note from Figure 3B that the mutation V32I causes the disappearance of the anticorrelated motion in the flap (R1 region). Additionally, V32I also strengthens the anticorrelated motion of residues 120–180 relative to residues 30–70. For the mutation G48V (Figure 3C), the anticorrelated motion in the flap (R1) is significantly strengthened, which shows that G48V induces a big conformational change in the flap region. According to Figure 3D, the mutation I50V strengthens the anticorrelated motion of residues 100–115 in chain B relative to residues 60–80. The mutation I54V induces the disappearance of the correlated and anticorrelated motions in the flap (R1) at the

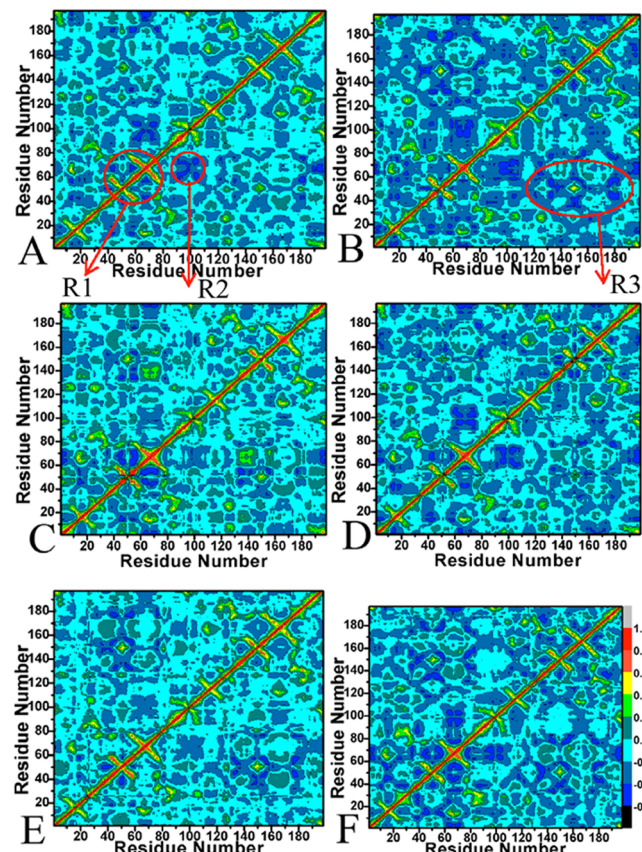


Figure 3. Cross-correlation matrices of the fluctuations of the coordinates for $\text{C}\alpha$ atoms around their corresponding mean positions after equilibration of the MD simulations: (A) WT; (B) V32I; (C) G48V; (D) I50V; (E) I54V; (F) I84V. The extents of correlated and anticorrelated motions are color-coded.

same time and also produces the anticorrelated movement between residues 120–180 and the flap (Figure 3E). As shown in Figure 3F, I84V not only greatly strengthens the anticorrelated motion in the flap but also generates strong anticorrelated motion between the wide region of residues 120–185 and the flap (R1). The mutations G48V, I50V, and I54V occur in the flaps and can directly induce conformational changes of the flaps. Although the mutations V32I and I84V are not located in the flaps, they also significantly affect the conformational changes of the flaps by a series of conformational alternation, which is supported by the increase in anticorrelated motion over a wide range (Figure 3B,F). The above analyses indicate that the change of the flap conformation may be the main origin of drug resistance of mutations toward APV. The results reported here are in good agreement with those of the RMSF analysis.

Free energy landscapes were constructed using the backbone ψ and φ angles to study the effect of mutation on conformational changes (Figure 4). According to Figure 4, although the mutation V32I does not obviously change its backbone ψ and φ angles (Figure 4A,B), the increase in the side-chain length must affect the conformation of the nearby residues, which is supported by the cross-correlation analysis (Figure 3B). The mutations G48V and I50V generate obvious changes in the free energy landscape based on their backbone ψ and φ angles relative to those in WT PR. As G48V and I50V are located in the flap region of PR, these changes must lead to

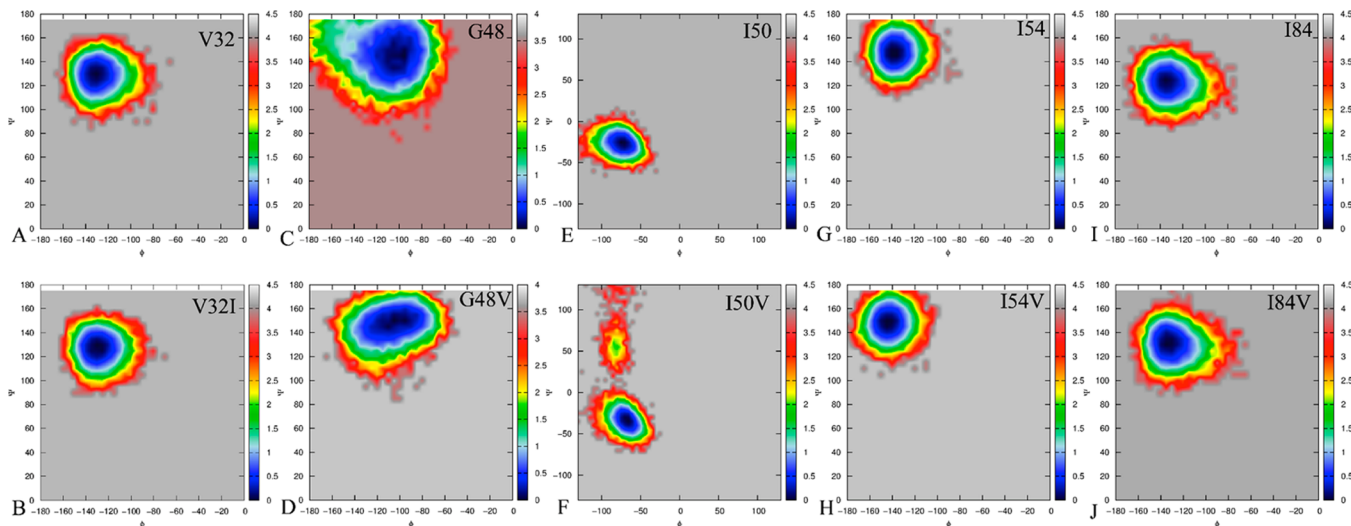


Figure 4. Contour maps of the free energy as a function of the backbone angles ψ and φ . Panels A, C, E, H, and I describe the WT residues, and panels B, D, F, H, and J describe the mutated residues.

Table 3. Main Hydrogen-Bonding Interactions Involved in APV Binding

hydrogen bond ^a	WT	V32I	G48V	I50V	I54V	I84V	occupancy (%) ^b
OD1@Asp25···O3-H@APV	98.95	95.43	8.94	20.23	89.45	26.06	
O@Asp30···N-H31@APV	97.71	85.24	88.43	49.76	91.12	46.75	
O@Wat301···N-H@Ile50	97.56	85.01	96.89	67.36	95.27	96.42	
O3@APV···HD2@Asp25'	70.45	10.0	18.08	9.84	60.04	9.00	
O5@APV···O-H1@Wat301	44.32	9.82	4.13	3.89	12.42	19.32	
O2@APV···O-H2@Wat301	30.22	71.52	66.08	36.33	66.21	60.50	
O6@APV···N-H@Asp29'	34.34	12.02	80.72	40.52	75.43	58.53	
O@Wat301···N-H@Ile50'	34.44	32.31	91.42	65.48	88.45	94.20	
O@Gly27'···N1-H@APV	9.75	7.01	7.06	5.11	12.25	50.53	
O6@APV···N-H@Asp30'	4.73	15.22	10.31	9.81	15.42	56.42	

^aThe hydrogen bonds are determined by an acceptor···donor distance of <3.5 Å and an acceptor···H–donor angle of >120°. ^bOccupancy is defined as the percentage of simulation time that a specific hydrogen bond exists.

the internal dynamics changes of the flap and the redistribution of their nearby residues (Figure 4C–F). Figure 4G,H suggests that the backbone φ angle of residue 54 undergoes an obvious change, as it is increased by 12° relative to Ile54. The mutation I54V, which occurs in the flaps, shortens the size of residue 54 and changes the shape of the flap, which must also produce a significant impact on the flap dynamics. The mutation I84V produces an increase of ~9° in ψ relative to WT PR (Figure 4A,B,J,J), which may induce conformation changes of its nearby residues. On the basis of the C_2 symmetry, the effect of mutations in chain B on the internal dynamics should be similar to the above analysis for chain A. These results are supported by the results of the RMSF and cross-correlation analyses.

Hydrogen-Bonding Interactions. To reveal changes in interactions between APV and PRs caused by mutations, hydrogen bond (HB) analysis was performed on the MD trajectory. The occupancies of HBs are listed in Table 3, and the structural information is depicted in Figure 5 using the lowest-energy structure from the MD simulations. Table 3 reveals that mutations produce an obvious impact on the hydrogen-bonding network formed by APV and PR. In the WT system, the bridging water Wat301 forms a tetrahedral arrangement of hydrogen bonds connecting the amide nitrogen atoms of Ile50/Ile50' with the sulfonamide oxygen and the

carbamate carbonyl oxygen in APV (Figure 5). As can be seen, the Wat301···O5@APV hydrogen bond is greatly decreased by

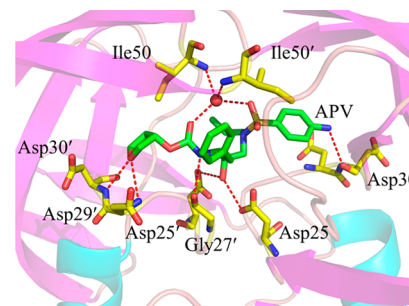


Figure 5. Hydrogen bonds formed between APV and separate residues in WT PR, represented by the red dashed lines. APV and the key residues are displayed in stick mode, and Wat301 is shown in ball mode.

mutations relative to the WT–APV complex, especially for the mutations V32I, G48V, and I50V. However, all five mutations increase the occupancy of the Wat301···O2@APV hydrogen bond. The two hydrogen bonds formed by Wat301 and residues Ile50/Ile50' are basically retained during the MD simulations.

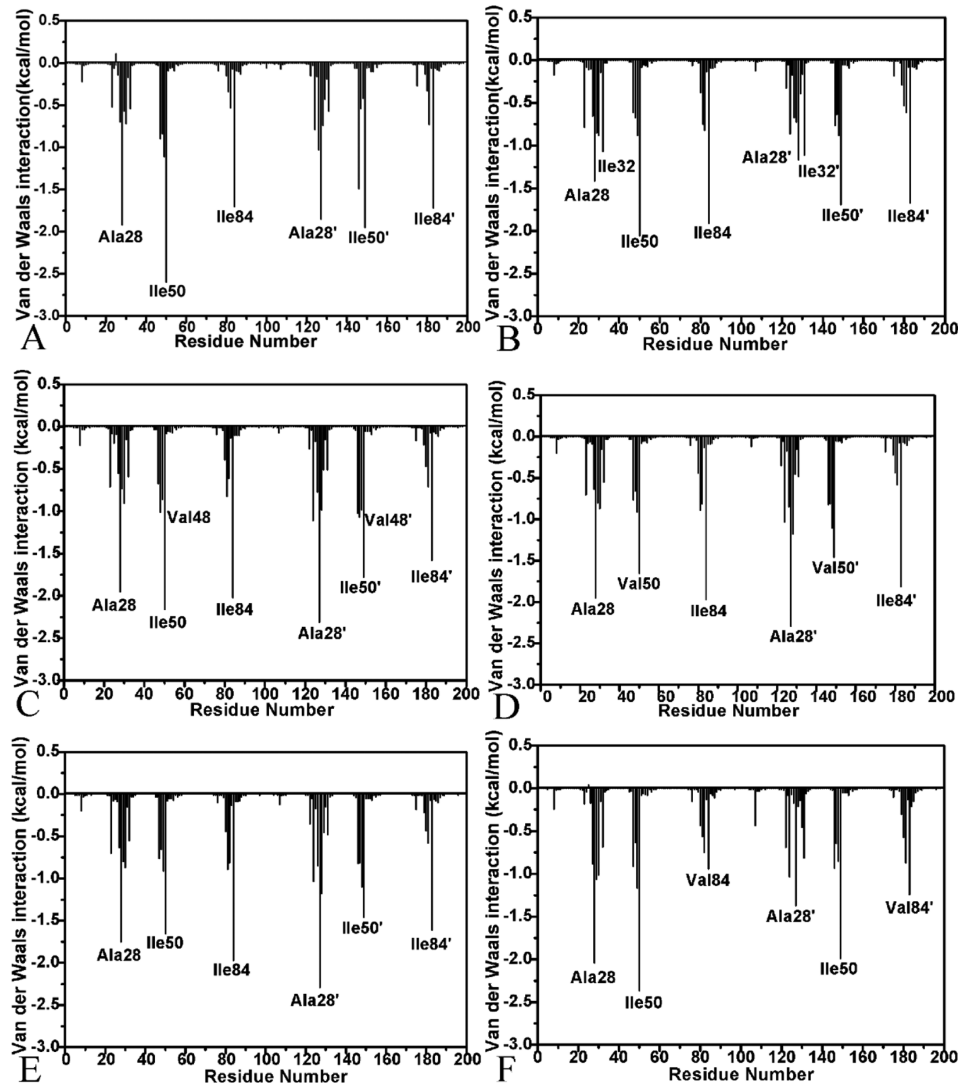


Figure 6. Van der Waals interactions of APV with separate residues in WT and mutant PR: (A) WT PR; (B) V32I mutant; (C) G48V mutant; (D) I50V mutant; (E) I54V mutant; (F) I84V mutant.

According to **Table 3** and **Figure 5**, APV forms six hydrogen bonds with WT PR. The occupancy of the two hydrogen bonds OD1@Asp25…O3-H@APV and O@Asp30…N-H31@APV are 98.95 and 97.71, respectively, and all five of the mutations lead to obvious decreases in the occupancies of these two hydrogen bonds during the MD simulations. Compared with the APV–WT PR complex, the occupancy of the O3@APV…HD2@Asp25' hydrogen bond is also obviously decreased. All of the mutations except V32I increase the occupancy of the O6@APV…N-H@Asp29' hydrogen bond. As shown in **Table 3**, the occupancies of the hydrogen bonds O@Gly27’…N1-H@APV and O6@APV…NH@Asp30' in the V32I, G48V, I50V, and I54V mutant complexes are similar to those in the WT complex, and only the mutation I84V increases the occupancies of these two HBs. On the basis of the above analyses, although mutation changes the stabilities of the HBs during the MD simulation, most of these HBs are basically conserved, which may explain why the alteration of the HBs provides only a weak contribution to drug resistance.

Analysis of van der Waals Interactions. The TI and MM-PBSA calculations imply that the decrease in van der Waals interactions caused by mutations contribute the main

force to drug resistance toward APV. To identify the molecular basis for this, the van der Waals interactions between APV and residues in PRs were computed using the equation

$$\Delta E_{vdW} = \sum \left(\frac{A_{ij}}{R_{ij}^{12}} - \frac{B_{ij}}{R_{ij}^6} \right) \quad (6)$$

where the parameters A_{ij} and B_{ij} arise from the Amber ff99SB force field. This equation has been applied to study other inhibitor–protein interactions.^{74,79,80} **Figure 6** presents the van der Waals interaction spectra of APV with separate residues in PR, and **Figure 7** depicts the position of APV relative to the key residues in the lowest-energy structure of the APV–PR complex from the MD simulations. According to **Figure 6**, the interaction spectra of the six complexes are quite similar overall. The favorable residues mainly arise from six groups around Ala28/Ala28', Ile50/Ile50', and Ile84/Ile84'.

In the APV–WT PR complex, the van der Waals interaction between Ala28 and APV is -2.01 kcal/mol , which mostly comes from the interaction of the hydrophobic ring R3 of APV with the alkyl group of Ala28⁸¹ (**Figure 7**). Similarly, the interaction between the hydrophobic ring R2 of APV and the

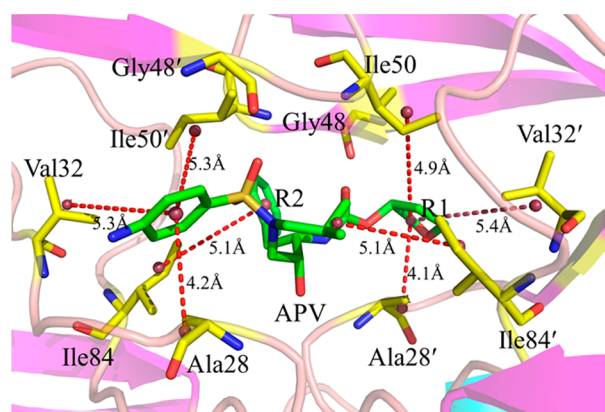


Figure 7. Van der Waals interactions between APV and separate hydrophobic residues in WT PR. The dashed lines represent CH- π and CH-CH interactions. APV is displayed in ball-and-stick mode, and the key residues are shown in stick mode.

alkyl group of Ala28' also provides a contribution of -1.89 kcal/mol to the binding affinity. Residues Ile50 and Ile50' form strong van der Waals interactions with APV (-2.64 and -1.98 kcal/mol, respectively), which arise from the interactions of the alkyls in Ile50/Ile50' with the hydrophobic rings R1 and R3 of APV, respectively. According to Figure 6A, the van der Waals interaction of residue Ile84 with APV is -1.81 kcal/mol, which structurally agrees with the interactions between the alkyl group of Ile84 and APV (Figure 7). Residue Ile84' forms a strong van der Waals interaction of -1.84 kcal/mol with APV that is mostly contributed by the interaction between the alkyl group of Ile84' and the hydrophobic ring R2. As shown in Figure 6A, the van der Waals interactions of APV with the two residues Val32 and Gly48 involved in mutations are weaker than -0.73 kcal/mol.

The mutation V32I enlarges the size of the hydrophobic side chain in residues 32 and 32', which correspondingly changes their van der Waals contacts with APV. As shown in Figure 6B, although the van der Waals interactions of the mutations V32I and V32'I with APV are decreased by 0.48 and 0.61 kcal/mol, this mutation also leads to a total increase of 2.53 kcal/mol in the van der Waals interactions of Ala28/Ala28' and Ile50/Ile50' with APV. This may be due to the changes in the positions of Ala28/Ala28' and Ile50/Ile50' relative to the hydrophobic groups of APV induced by the increase in the size of the side chain caused by the V32I mutation. This result is supported by the experimental studies by Shen et al.¹² Mutation of Gly to Val, which adds one methyl group, can reduce the volume of the flap region and alter the hydrophobic interactions in the cluster near this mutation. Thus, one can observe from panels C and A in Figure 6 that although the mutation G48V leads to small decreases of 0.14 and 0.39 kcal/mol in the van der Waals interactions of V48 and V48', respectively, with APV, it also produces a total increase of 0.61 kcal/mol in the van der Waals interactions of Ile50/Ile50' with APV. Figure 6A suggests that residues Ile54 and Ile54' do not directly interact with APV. The mutation of Ile to Val, which removes one methyl group, can increase the volume of the flap region and change the hydrophobic interactions in the cluster around Ile54/Ile54'. The comparison of Figure 6E with Figure 6A shows that the mutation I54V induces a total decrease of 1.50 kcal/mol in the van der Waals interactions between Ile50/Ile50' and APV. Mutation from Ile to Val also shrinks the binding pockets of Ile50/Ile50' and Ile84/Ile84', which

correspondingly reduces the number of hydrophobic contacts with APV and alters their hydrophobic interactions with APV. Figure 6D indicates that the van der Waals interactions of residues 50 and 50' with APV are decreased by 1.47 kcal/mol due to the mutation I50V, and Figure 6F proves that the I84V/I84'V mutations result in a total decrease of 1.18 kcal/mol in the van der Waals interactions between APV and residues 84 and 84'. The above results basically agree with those of previous computational and experimental studies.^{12,17,40}

On the basis of the above analysis, although mutations with larger side chains (V32I and G48V) strengthen the van der Waals interactions with APV, they also induce conformation changes of their adjacent residues and flaps that can decrease the hydrophobic contacts between these regions and APV. Mutations with smaller side chains (I50V, I54V, and I84V) cause losses of internal hydrophobic interactions in the binding complexes. Overall, the structural adjustments of the five mutated residues induce decreases in the van der Waals interactions. Moreover, the decreases in the van der Waals interactions between the key residues and APV provide the main contributions to drug resistance of mutations toward APV.

CONCLUSIONS

In this work, MD simulations and binding free energy calculations were combined to probe the drug resistance mechanism of the five mutations V32I, G48V, I50V, I54V, and I84V in HIV-1 protease toward the inhibitor APV. Results of thermodynamic integration calculations indicate that these mutations strongly influence the van der Waals interactions between mutated PRs and APV, which implies that the change in the van der Waals interactions is the main driving force for drug resistance. These results are further supported by the calculations using the MM-PBSA method. Dynamics analysis further shows that the structural adjustment of the mutated residues induces changes in their positions relative to the hydrophobic groups of APV. These changes in their relative positions not only reduce van der Waals interactions between mutated PR and APV but also generate an obvious effect on the stability of hydrogen bonds in the binding pocket. The energetic and dynamic information obtained in the current studies could provide important guidance for the design of new potent inhibitors that could alleviate drug resistance of PR due to mutations.

ASSOCIATED CONTENT

Supporting Information

The Supporting Information is available free of charge on the ACS Publications website at DOI: [10.1021/acs.jcim.5b00173](https://doi.org/10.1021/acs.jcim.5b00173).

Figures S1–S3 and Table S1 (PDF)

AUTHOR INFORMATION

Corresponding Authors

*E-mail: chenjianzhong1970@163.com (J.C.).

*E-mail: zhtutong@itcs.ecnu.edu.cn (T.Z.).

Notes

The authors declare no competing financial interest.

ACKNOWLEDGMENTS

This work was supported by the National Natural Science Foundation of China (21433004, 21403068, and 11274206), a China Postdoctoral Science Foundation funded project

(2014MS61434), a Shandong Province University Science and Technology project (J14LJ07), and the Dr. Start-up Foundation of Shandong Jiaotong University.

■ REFERENCES

- (1) Navia, M. A.; Fitzgerald, P. M.; McKeever, B. M.; Leu, C.-T.; Heimbach, J. C.; Herber, W. K.; Sigal, I. S.; Darke, P. L.; Springer, J. P. Three-Dimensional Structure of Aspartyl Protease from Human Immunodeficiency Virus HIV-1. *Nature* **1989**, *337*, 615–620.
- (2) Lapatto, R.; Blundell, T.; Hemmings, A.; Overington, J.; Wilderspin, A.; Wood, S.; Merson, J. R.; Whittle, P. J.; Danley, D. E.; Geoghegan, K. F.; Hawrylik, S. J.; Lee, S. E.; Scheld, K. G.; Hobart, P. M. X-Ray Analysis of HIV-1 Proteinase at 2.7 Å Resolution Confirms Structural Homology among Retroviral Enzymes. *Nature* **1989**, *342*, 299–302.
- (3) Ishima, R.; Freedberg, D. I.; Wang, Y.-X.; Louis, J. M.; Torchia, D. A. Flap Opening and Dimer-Interface Flexibility in the Free and Inhibitor-Bound HIV Protease, and Their Implications for Function. *Structure* **1999**, *7*, 1047–1055.
- (4) Scott, W. R.; Schiffer, C. A. Curling of Flap Tips in HIV-1 Protease as a Mechanism for Substrate Entry and Tolerance of Drug Resistance. *Structure* **2000**, *8*, 1259–1265.
- (5) Carr, A.; Samaras, K.; Chisholm, D. J.; Cooper, D. A. Pathogenesis of HIV-1-Protease Inhibitor-Associated Peripheral Lipodystrophy, Hyperlipidaemia, and Insulin Resistance. *Lancet* **1998**, *351*, 1881–1883.
- (6) Judd, D. A.; Nettles, J. H.; Nevins, N.; Snyder, J. P.; Liotta, D. C.; Tang, J.; Ermolieff, J.; Schinazi, R. F.; Hill, C. L. Polyoxometalate HIV-1 Protease Inhibitors. A New Mode of Protease Inhibition. *J. Am. Chem. Soc.* **2001**, *123*, 886–897.
- (7) Kovalevsky, A. Y.; Liu, F.; Leshchenko, S.; Ghosh, A. K.; Louis, J. M.; Harrison, R. W.; Weber, I. T. Ultra-High Resolution Crystal Structure of HIV-1 Protease Mutant Reveals Two Binding Sites for Clinical Inhibitor TMC114. *J. Mol. Biol.* **2006**, *363*, 161–173.
- (8) Wlodawer, A.; Vondrasek, J. Inhibitors of HIV-1 Protease: A Major Success of Structure-Assisted Drug Design 1. *Annu. Rev. Biophys. Biomol. Struct.* **1998**, *27*, 249–284.
- (9) Ghosh, A. K.; Chapsal, B. D.; Weber, I. T.; Mitsuya, H. Design of HIV Protease Inhibitors Targeting Protein Backbone: An Effective Strategy for Combating Drug Resistance. *Acc. Chem. Res.* **2008**, *41*, 78–86.
- (10) Williams, G. C.; Sinko, P. J. Oral Absorption of the HIV Protease Inhibitors: A Current Update. *Adv. Drug Delivery Rev.* **1999**, *39*, 211–238.
- (11) Kim, E.; Baker, C.; Dwyer, M.; Murcko, M.; Rao, B.; Tung, R.; Navia, M. Crystal Structure of HIV-1 Protease in Complex with VX-478, a Potent and Orally Bioavailable Inhibitor of the Enzyme. *J. Am. Chem. Soc.* **1995**, *117*, 1181–1182.
- (12) Shen, C. H.; Wang, Y. F.; Kovalevsky, A. Y.; Harrison, R. W.; Weber, I. T. Amprenavir Complexes with HIV-1 Protease and Its Drug-Resistant Mutants Altering Hydrophobic Clusters. *FEBS J.* **2010**, *277*, 3699–3714.
- (13) Surleraux, D. L.; Tahri, A.; Verschueren, W. G.; Pille, G. M.; De Kock, H. A.; Jonckers, T. H.; Peeters, A.; De Meyer, S.; Azijn, H.; Pauwels, R.; de Bethune, M.-P.; King, N. M.; Prabu-Jeyabalan, M.; Schiffer, C. A.; Wigerinck, P. B. T. P. Discovery and Selection of TMC114, a Next Generation HIV-1 Protease Inhibitor. *J. Med. Chem.* **2005**, *48*, 1813–1822.
- (14) Chen, Z.; Li, Y.; Chen, E.; Hall, D. L.; Darke, P. L.; Culberson, C.; Shafer, J. A.; Kuo, L. C. Crystal Structure at 1.9-Å Resolution of Human Immunodeficiency Virus (HIV) II Protease Complexed with L-735, an Orally Bioavailable Inhibitor of the HIV Proteases. *J. Biol. Chem.* **1994**, *269*, 26344–26348.
- (15) Meher, B. R.; Wang, Y. Interaction of I50V Mutant and I50L/A71V Double Mutant HIV-Protease with Inhibitor TMC114 (Darunavir): Molecular Dynamics Simulation and Binding Free Energy Studies. *J. Phys. Chem. B* **2012**, *116*, 1884–1900.
- (16) Hou, T.; McLaughlin, W. A.; Wang, W. Evaluating the Potency of HIV-1 Protease Drugs to Combat Resistance. *Proteins: Struct., Funct., Genet.* **2008**, *71*, 1163–1174.
- (17) Leonis, G.; Steinbrecher, T.; Papadopoulos, M. G. A Contribution to the Drug Resistance Mechanism of Darunavir, Amprenavir, Indinavir, and Saquinavir Complexes with HIV-1 Protease Due to Flap Mutation I50V: A Systematic MM-PBSA and Thermodynamic Integration Study. *J. Chem. Inf. Model.* **2013**, *53*, 2141–2153.
- (18) Johnson, V. A.; Brun-Vézinet, F.; Clotet, B.; Kuritzkes, D. R.; Pillay, D.; Schapiro, J. M.; Richman, D. D. Update of the Drug Resistance Mutations in HIV-1: Fall 2006. *Top. HIV Med.* **2006**, *14*, 125–130.
- (19) Chen, J.; Zhang, S.; Liu, X.; Zhang, Q. Insights into Drug Resistance of Mutations D30N and I50V to HIV-1 Protease Inhibitor TMC-114: Free Energy Calculation and Molecular Dynamic Simulation. *J. Mol. Model.* **2010**, *16*, 459–468.
- (20) Kovalevsky, A. Y.; Chumanovich, A. A.; Liu, F.; Louis, J. M.; Weber, I. T. Caught in the Act: The 1.5 Å Resolution Crystal Structures of the HIV-1 Protease and the I54V Mutant Reveal a Tetrahedral Reaction Intermediate. *Biochemistry* **2007**, *46*, 14854–14864.
- (21) Borman, A. M.; Paulous, S.; Clavel, F. Resistance of Human Immunodeficiency Virus Type 1 to Protease Inhibitors: Selection of Resistance Mutations in the Presence and Absence of the Drug. *J. Gen. Virol.* **1996**, *77*, 419–426.
- (22) Duan, R.; Lazim, R.; Zhang, D. Understanding the Basis of I50V-Induced Affinity Decrease in HIV-1 Protease Via Molecular Dynamics Simulations Using Polarized Force Field. *J. Comput. Chem.* **2015**, *36*, 1885.
- (23) Liu, F.; Kovalevsky, A. Y.; Louis, J. M.; Boross, P. I.; Wang, Y.-F.; Harrison, R. W.; Weber, I. T. Mechanism of Drug Resistance Revealed by the Crystal Structure of the Unliganded HIV-1 Protease with F53L Mutation. *J. Mol. Biol.* **2006**, *358*, 1191–1199.
- (24) Pazhanisamy, S.; Stuver, C. M.; Cullinan, A. B.; Margolin, N.; Rao, B.; Livingston, D. J. Kinetic Characterization of Human Immunodeficiency Virus Type-1 Protease-Resistant Variants. *J. Biol. Chem.* **1996**, *271*, 17979–17985.
- (25) Liu, F.; Kovalevsky, A. Y.; Tie, Y.; Ghosh, A. K.; Harrison, R. W.; Weber, I. T. Effect of Flap Mutations on Structure of HIV-1 Protease and Inhibition by Saquinavir and Darunavir. *J. Mol. Biol.* **2008**, *381*, 102–115.
- (26) Alcaro, S.; Artese, A.; Ceccherini-Silberstein, F.; Ortuso, F.; Perno, C. F.; Sing, T.; Svicher, V. Molecular Dynamics and Free Energy Studies on the Wild-Type and Mutated HIV-1 Protease Complexed with Four Approved Drugs: Mechanism of Binding and Drug Resistance. *J. Chem. Inf. Model.* **2009**, *49*, 1751–1761.
- (27) Hu, G.-D.; Zhu, T.; Zhang, S.-L.; Wang, D.; Zhang, Q.-G. Some Insights into Mechanism for Binding and Drug Resistance of Wild Type and I50V V82A and I84V Mutations in HIV-1 Protease with GRL-98065 Inhibitor from Molecular Dynamic Simulations. *Eur. J. Med. Chem.* **2010**, *45*, 227–235.
- (28) Kar, P.; Knecht, V. Energetic Basis for Drug Resistance of HIV-1 Protease Mutants against Amprenavir. *J. Comput.-Aided Mol. Des.* **2012**, *26*, 215–232.
- (29) Antunes, D. A.; Rigo, M. M.; Sinigaglia, M.; de Medeiros, R. M.; Junqueira, D. M.; Almeida, S. E.; Vieira, G. F. New Insights into the in Silico Prediction of HIV Protease Resistance to Nelfinavir. *PLoS One* **2014**, *9*, e87520.
- (30) Wittayanarakul, K.; Aruksakunwong, O.; Saen-oon, S.; Chantratita, W.; Parasuk, V.; Sompornpisut, P.; Hannongbua, S. Insights into Saquinavir Resistance in the G48V HIV-1 Protease: Quantum Calculations and Molecular Dynamic Simulations. *Biophys. J.* **2005**, *88*, 867–879.
- (31) Rhee, S.-Y.; Taylor, J.; Fessel, W. J.; Kaufman, D.; Towner, W.; Troia, P.; Ruane, P.; Hellinger, J.; Shirvani, V.; Zolopa, A.; Shafer, R. W. HIV-1 Protease Mutations and Protease Inhibitor Cross-Resistance. *Antimicrob. Agents Chemother.* **2010**, *54*, 4253–4261.

- (32) Paulsen, D.; Elston, R.; Snowden, W.; Tisdale, M.; Ross, L. Differentiation of Genotypic Resistance Profiles for Amprenavir and Lopinavir, a Valuable Aid for Choice of Therapy in Protease Inhibitor-Experienced HIV-1-Infected Subjects. *J. Antimicrob. Chemother.* **2003**, *S2*, 319–323.
- (33) Wu, R.; Hu, P.; Wang, S.; Cao, Z.; Zhang, Y. Flexibility of Catalytic Zinc Coordination in Thermolysin and HDAC8: A Born–Oppenheimer Ab Initio QM/MM Molecular Dynamics Study. *J. Chem. Theory Comput.* **2010**, *6*, 337–343.
- (34) Wang, J.; Fulford, T.; Shao, Q.; Javelle, A.; Yang, H.; Zhu, W.; Merrick, M. Ammonium Transport Proteins with Changes in One of the Conserved Pore Histidines Have Different Performance in Ammonia and Methylamine Conduction. *PLoS One* **2013**, *8*, e62745.
- (35) Wu, E. L.; Wong, K.-Y.; Zhang, X.; Han, K.; Gao, J. Determination of the Structure Form of the Fourth Ligand of Zinc in Acutolysin a Using Combined Quantum Mechanical and Molecular Mechanical Simulation. *J. Phys. Chem. B* **2009**, *113*, 2477–2485.
- (36) Zhu, T.; Xiao, X.; Ji, C.; Zhang, J. Z. A New Quantum Calibrated Force Field for Zinc–Protein Complex. *J. Chem. Theory Comput.* **2013**, *9*, 1788–1798.
- (37) Zhang, Q.; Xu, Z.; Liang, J.; Pei, J.; Sun, H. Structural and Magnetic Properties of Sr₂FeMoO₆ Film Prepared by Electrophoresis Technique. *J. Magn. Magn. Mater.* **2014**, *354*, 231–234.
- (38) Tong, C.; Lin, X.; Yang, Y.; Hou, Z. D. 1)-Total Labellings of Regular Nonbipartite Graphs and an Application to Flower Snarks. *Ars Combinatoria* **2010**, *XCVI*, 33–40.
- (39) Duan, L. L.; Mei, Y.; Zhang, Q. G.; Zhang, J. Z. Intra-Protein Hydrogen Bonding Is Dynamically Stabilized by Electronic Polarization. *J. Chem. Phys.* **2009**, *130*, 115102.
- (40) Tzoupis, H.; Leonis, G.; Mavromoustakos, T.; Papadopoulos, M. G. A Comparative Molecular Dynamics, MM–PBSA and Thermodynamic Integration Study of Saquinavir Complexes with Wild-Type HIV-1 PR and L10I, G48V, L63P, A71V, G73S, V82A and I84V Single Mutants. *J. Chem. Theory Comput.* **2013**, *9*, 1754–1764.
- (41) Chen, J.; Wang, J.; Zhu, W. Binding Modes of Three Inhibitors 8CA, F8A and I4A to A-FABP Studied Based on Molecular Dynamics Simulation. *PLoS One* **2014**, *9*, e99862.
- (42) Wu, E. L.; Han, K. L.; Zhang, J. Z. H. Selectivity of Neutral/Weakly Basic P1 Group Inhibitors of Thrombin and Trypsin by a Molecular Dynamics Study. *Chem. - Eur. J.* **2008**, *14*, 8704–8714.
- (43) Gao, Y.; Lu, X.; Duan, L. L.; Zhang, J. Z.; Mei, Y. Polarization of Intraprotein Hydrogen Bond Is Critical to Thermal Stability of Short Helix. *J. Phys. Chem. B* **2012**, *116*, 549–554.
- (44) Zhu, T.; He, X.; Zhang, J. Z. Fragment Density Functional Theory Calculation of NMR Chemical Shifts for Proteins with Implicit Solvation. *Phys. Chem. Chem. Phys.* **2012**, *14*, 7837–7845.
- (45) Wang, J.; Yang, H.; Zuo, Z.; Yan, X.; Wang, Y.; Luo, X.; Jiang, H.; Chen, K.; Zhu, W. Molecular Dynamics Simulations on the Mechanism of Transporting Methylamine and Ammonia by Ammonium Transporter Amtb. *J. Phys. Chem. B* **2010**, *114*, 15172–15179.
- (46) Hu, G.; Wang, J. Ligand Selectivity of Estrogen Receptors by a Molecular Dynamics Study. *Eur. J. Med. Chem.* **2014**, *74*, 726–735.
- (47) Duan, L. L.; Mei, Y.; Zhang, D.; Zhang, Q. G.; Zhang, J. Z. H. Folding of a Helix at Room Temperature Is Critically Aided by Electrostatic Polarization of Intraprotein Hydrogen Bonds. *J. Am. Chem. Soc.* **2010**, *132*, 11159–11164.
- (48) Xu, Y.; Wang, R. A Computational Analysis of the Binding Affinities of FKBP12 Inhibitors Using the MM PB/SA Method. *Proteins: Struct., Funct., Genet.* **2006**, *64*, 1058–1068.
- (49) Wang, J.; Morin, P.; Wang, W.; Kollman, P. A. Use of MM-PBSA in Reproducing the Binding Free Energies to HIV-1 Rt of Tibo Derivatives and Predicting the Binding Mode to HIV-1 RT of Efavirenz by Docking and MM-PBSA. *J. Am. Chem. Soc.* **2001**, *123*, 5221–5230.
- (50) Wang, W.; Kollman, P. A. Free Energy Calculations on Dimer Stability of the HIV Protease Using Molecular Dynamics and a Continuum Solvent Model. *J. Mol. Biol.* **2000**, *303*, 567–582.
- (51) Wang, W.; Kollman, P. A. Computational Study of Protein Specificity: The Molecular Basis of HIV-1 Protease Drug Resistance. *Proc. Natl. Acad. Sci. U. S. A.* **2001**, *98*, 14937–14942.
- (52) Straatsma, T.; Berendsen, H. Free Energy of Ionic Hydration: Analysis of a Thermodynamic Integration Technique to Evaluate Free Energy Differences by Molecular Dynamics Simulations. *J. Chem. Phys.* **1988**, *89*, 5876–5886.
- (53) Zacharias, M.; Straatsma, T.; McCammon, J. Separation-Shifted Scaling, a New Scaling Method for Lennard-Jones Interactions in Thermodynamic Integration. *J. Chem. Phys.* **1994**, *100*, 9025–9031.
- (54) Gouda, H.; Kuntz, I. D.; Case, D. A.; Kollman, P. A. Free Energy Calculations for Theophylline Binding to an RNA Aptamer: Comparison of MM PBSA and Thermodynamic Integration Methods. *Biopolymers* **2003**, *68*, 16–34.
- (55) King, N. M.; Prabu-Jeyabalan, M.; Bandaranayake, R. M.; Nalam, M. N.; Nalivaika, E. A.; Özen, A.; Haliloglu, T.; Yilmaz, N. K.; Schiffer, C. A. Extreme Entropy–Enthalpy Compensation in a Drug-Resistant Variant of HIV-1 Protease. *ACS Chem. Biol.* **2012**, *7*, 1536–1546.
- (56) Chen, J.; Yang, M.; Hu, G.; Shi, S.; Yi, C.; Zhang, Q. Insights into the Functional Role of Protonation States in the HIV-1 Protease-BEA369 Complex: Molecular Dynamics Simulations and Free Energy Calculations. *J. Mol. Model.* **2009**, *15*, 1245–1252.
- (57) Harte, W. E., Jr; Beveridge, D. L. Prediction of the Protonation State of the Active Site Aspartyl Residues in HIV-1 Protease-Inhibitor Complexes Via Molecular Dynamics Simulation. *J. Am. Chem. Soc.* **1993**, *115*, 3883–3886.
- (58) Li, H.; Robertson, A. D.; Jensen, J. H. Very Fast Empirical Prediction and Rationalization of Protein PKA Values. *Proteins: Struct., Funct., Genet.* **2005**, *61*, 704–721.
- (59) Bas, D. C.; Rogers, D. M.; Jensen, J. H. Very Fast Prediction and Rationalization of PKA Values for Protein–Ligand Complexes. *Proteins: Struct., Funct., Genet.* **2008**, *73*, 765–783.
- (60) Case, D. A.; Darden, T. A.; Cheatham, T. E., III; Simmerling, C. L.; Wang, J.; Duke, R. E.; Luo, R.; Walker, R. C.; Zhang, W.; Merz, K. M.; Roberts, S.; Hayik, S.; Roitberg, A.; Seabra, G.; Swails, J.; Götz, A. W.; Kolossvary, I.; Wong, K. F.; Paesani, F.; Vanicek, J.; Wolf, R. M.; Liu, J.; Wu, X.; Brozell, S. R.; Steinbrecher, T.; Gohlke, H.; Cai, Q.; Ye, X.; Wang, J.; Hsieh, M.-J.; Cui, G.; Roe, D. R.; Mathews, D. H.; Sestin, M. G.; Salomon-Ferrer, R.; Sagui, C.; Babin, V.; Luchko, T.; Gusarov, S.; Kovalenko, A.; Kollman, P. A. *Amber 12*; University of California: San Francisco, 2012.
- (61) Hornak, V.; Abel, R.; Okur, A.; Strockbine, B.; Roitberg, A.; Simmerling, C. Comparison of Multiple AMBER Force Fields and Development of Improved Protein Backbone Parameters. *Proteins: Struct., Funct., Genet.* **2006**, *65*, 712–725.
- (62) Frisch, M. J.; Trucks, G. W.; Schlegel, H. B.; Scuseria, G. E.; Robb, M. A.; Cheeseman, J. R.; Scalmani, G.; Barone, V.; Mennucci, B.; Petersson, G. A.; Nakatsuji, H.; Caricato, M.; Li, X.; Hratchian, H. P.; Izmaylov, A. F.; Bloino, J.; Zheng, G.; Sonnenberg, J. L.; Hada, M.; Ehara, M.; Toyota, K.; Fukuda, R.; Hasegawa, J.; Ishida, M.; Nakajima, T.; Honda, Y.; Kitao, O.; Nakai, H.; Vreven, T.; Montgomery, J. A., Jr.; Peralta, J. E.; Ogliaro, F.; Bearpark, M.; Heyd, J. J.; Brothers, E.; Kudin, K. N.; Staroverov, V. N.; Kobayashi, R.; Normand, J.; Raghavachari, K.; Rendell, A.; Burant, J. C.; Iyengar, S. S.; Tomasi, J.; Cossi, M.; Rega, N.; Millam, J. M.; Klene, M.; Knox, J. E.; Cross, J. B.; Bakken, V.; Adamo, C.; Jaramillo, J.; Gomperts, R.; Stratmann, R. E.; Yazev, O.; Austin, A. J.; Cammi, R.; Pomelli, C.; Ochterski, J. W.; Martin, R. L.; Morokuma, K.; Zakrzewski, V. G.; Voth, G. A.; Salvador, P.; Dannenberg, J. J.; Dapprich, S.; Daniels, A. D.; Farkas, Ö.; Foresman, J. B.; Ortiz, J. V.; Cioslowski, J.; Fox, D. J. *Gaussian 09*, revision C.01; Gaussian, Inc.: Wallingford, CT, 2009.
- (63) Wang, J.; Wolf, R. M.; Caldwell, J. W.; Kollman, P. A.; Case, D. A. Development and Testing of a General AMBER Force Field. *J. Comput. Chem.* **2004**, *25*, 1157–1174.
- (64) Jorgensen, W. L.; Chandrasekhar, J.; Madura, J. D.; Impey, R. W.; Klein, M. L. Comparison of Simple Potential Functions for Simulating Liquid Water. *J. Chem. Phys.* **1983**, *79*, 926–930.

- (65) Ryckaert, J.-P.; Ciccotti, G.; Berendsen, H. J. Numerical Integration of the Cartesian Equations of Motion of a System with Constraints: Molecular Dynamics of N-Alkanes. *J. Comput. Phys.* **1977**, *23*, 327–341.
- (66) Izaguirre, J. A.; Catarello, D. P.; Wozniak, J. M.; Skeel, R. D. Langevin Stabilization of Molecular Dynamics. *J. Chem. Phys.* **2001**, *114*, 2090–2098.
- (67) Darden, T.; York, D.; Pedersen, L. Particle Mesh Ewald: An N-Log (N) Method for Ewald Sums in Large Systems. *J. Chem. Phys.* **1993**, *98*, 10089–10092.
- (68) Essmann, U.; Perera, L.; Berkowitz, M. L.; Darden, T.; Lee, H.; Pedersen, L. G. A Smooth Particle Mesh Ewald Method. *J. Chem. Phys.* **1995**, *103*, 8577–8593.
- (69) Gohlke, H.; Kiel, C.; Case, D. A. Insights into Protein-Protein Binding by Binding Free Energy Calculation and Free Energy Decomposition for the Ras-Raf and Ras-Ralgds Complexes. *J. Mol. Biol.* **2003**, *330*, 891–913.
- (70) Xu, B.; Shen, H.; Zhu, X.; Li, G. Fast and Accurate Computation Schemes for Evaluating Vibrational Entropy of Proteins. *J. Comput. Chem.* **2011**, *32*, 3188–3193.
- (71) Ichiye, T.; Karplus, M. Collective Motions in Proteins: A Covariance Analysis of Atomic Fluctuations in Molecular Dynamics and Normal Mode Simulations. *Proteins: Struct., Funct., Genet.* **1991**, *11*, 205–217.
- (72) Steinbrecher, T.; Mobley, D. L.; Case, D. A. Nonlinear Scaling Schemes for Lennard-Jones Interactions in Free Energy Calculations. *J. Chem. Phys.* **2007**, *127*, 214108.
- (73) Kirkwood, J. G. Statistical Mechanics of Fluid Mixtures. *J. Chem. Phys.* **1935**, *3*, 300–313.
- (74) Chen, J.; Liang, Z.; Wang, W.; Yi, C.; Zhang, S.; Zhang, Q. Revealing Origin of Decrease in Potency of Darunavir and Amprenavir against HIV-2 Relative to HIV-1 Protease by Molecular Dynamics Simulations. *Sci. Rep.* **2014**, *4*, 6872.
- (75) Mittal, S.; Bandaranayake, R. M.; King, N. M.; Prabu-Jeyabalan, M.; Nalam, M. N.; Nalivaika, E. A.; Yilmaz, N. K.; Schiffer, C. A. Structural and Thermodynamic Basis of Amprenavir/Darunavir and Atazanavir Resistance in HIV-1 Protease with Mutations at Residue 50. *J. Virol.* **2013**, *87*, 4176–4184.
- (76) Virgil, S. C. First-Generation HIV-1 Protease Inhibitors for the Treatment of HIV/AIDS. In *Aspartic Acid Proteases as Therapeutic Targets*, 1st ed.; Ghosh, A. K., Mannhold, R., Kubinyi, H., Folkers, G., Eds.; Wiley-VCH: Weinheim, Germany, 2011; pp 139–168.
- (77) Redshaw, S.; Roberts, N. A.; Thomas, N. G. The Road to Fortovase. A History of Saquinavir, the First Human Immunodeficiency Virus Protease Inhibitor. In *Proteases as Targets for Therapy*, 1st ed.; Von der Helm, K., Korant, B. D., Cheronis, J. C., Eds.; Springer: Berlin, 2000; pp 3–21.
- (78) Roe, D. R.; Cheatham, T. E., III Ptraj and Cpptraj: Software for Processing and Analysis of Molecular Dynamics Trajectory Data. *J. Chem. Theory Comput.* **2013**, *9*, 3084–3095.
- (79) Ding, Y.; Mei, Y.; Zhang, J. Z. Quantum Mechanical Studies of Residue-Specific Hydrophobic Interactions in P53–MDM2 Binding. *J. Phys. Chem. B* **2008**, *112*, 11396–11401.
- (80) Chen, J.; Wang, J.; Zhang, Q.; Chen, K.; Zhu, W. A Comparative Study of Trypsin Specificity Based on QM/MM Molecular Dynamics Simulation and QM/MM GBsa Calculation. *J. Biomol. Struct. Dyn.* **2015**, *1*.
- (81) Nishio, M.; Umezawa, Y.; Fantini, J.; Weiss, M. S.; Chakrabarti, P. Ch- π Hydrogen Bonds in Biological Macromolecules. *Phys. Chem. Chem. Phys.* **2014**, *16*, 12648–12683.